Single-Shot Diagnosis of Electron Energy Evolution via Streaked Betatron X Rays in a Curved Laser Wakefield Accelerator

Y. Ma,[1,*] J. A. Cardarelli,[1] P. T. Campbell,[1] S. Fourmaux,[2] R. Fitzgarrald,[1] M. D. Balcazar,[1] A. F. Antoine,[1] N. F. Beier,[3] Q. Qian,[1] A. E. Hussein,[3] B. Kettle,[4] S. R. Klein,[1] K. Krushelnick,[1] Y. F. Li,[5] S. P. D. Mangles,[4] G. Sarri,[6] D. Seipt,[7,8] V. Senthilkumaran,[3] M. J. V. Streeter,[6] L. Willingale,[1] and A. G. R. Thomas[1]

[1]*Gérard Mourou Center for Ultrafast Optical Science, University of Michigan, Ann Arbor, Michigan 48109-2099, USA*
[2]*Institut National de la Recherche Scientifique - Énergie, Matériaux et Télécommunications, Université du Québec (INRS-EMT), 1650 Lionel Boulet, Varennes, Québec J3X 1P7, Canada*
[3]*Department of Electrical and Computer Engineering, University of Alberta, Edmonton, Alberta T6G 1H9, Canada*
[4]*The John Adams Institute for Accelerator Science, Imperial College London, London SW7 2AZ, United Kingdom*
[5]*Institute of Physics, Chinese Academy of Sciences, Beijing 100190, China*
[6]*School of Mathematics and Physics, Queen's University Belfast, Belfast BT7 1NN, United Kingdom*
[7]*Helmholtz Institut Jena, Fröbelstieg 3, Jena 07743, Germany*
[8]*GSI Helmholtzzentrum für Schwerionenforschung GmbH, Planckstraße 1, 64291 Darmstadt, Germany*

(Received 19 November 2023; revised 7 March 2024; accepted 2 May 2024; published 31 May 2024)

We report on an experimental observation of the streaking of betatron x rays in a curved laser wakefield accelerator. The streaking of the betatron x rays was realized by launching a laser pulse into a plasma with a transverse density gradient. By controlling the plasma density and the density gradient, we realized the steering of the laser driver, electron beam, and betatron x rays simultaneously. Moreover, we observed an energy-angle correlation of the streaked betatron x rays and utilized it in diagnosing the electron acceleration process in a single-shot mode. Our work could also find applications in advanced control of laser beam and particle propagation. More importantly, the angular streaked betatron x ray has an intrinsic spatiotemporal correlation, which makes it a promising tool for single-shot pump-probe applications.

DOI: 10.1103/PhysRevLett.132.225001

Laser wakefield acceleration (LWFA) [1] has gained much attention as a promising alternative to large-scale radio-frequency accelerators due to its larger acceleration gradient. It has demonstrated the capability for generating multi-GeV electron beams [2–6], as well as its success in practical applications in various science frontiers, such as advanced light sources [7,8] including compact x ray free electron lasers [9,10] and strong field quantum electrodynamics [11,12]. A long-term goal of laser plasma accelerators is to reach energies and beam quality suitable for future TeV electron-positron colliders [13]. In practice, however, the maximum energy gain of a LWFA has been only of order $E \leq 10$ GeV limited by the so-called "3D" problem [14], i.e., *diffraction*, *depletion*, and *dephasing*. Therefore, to achieve TeV energy gain, multistage LWFA [15] and dephasingless LWFA [16–18] have been proposed. In either case, it is essential to precisely diagnose the electron acceleration process to maximize the electron energy gain.

So far, the diagnosis of the electron spectrum is primarily performed with magnetic electron spectrometers located downstream of the accelerator. Because the electron spectrum was measured after the whole acceleration process, this causes the issue that it provides no information of the electron energy evolution. Attempts to make measurements of such evolution have been made in the multishot mode by either varying the acceleration length [7,19–23] or by inferring from the Thomson scattering spectrum in which the tunable colliding location was inside the accelerator in a noninvasive mode [24]. Such multishot methods critically relay on the stability and reproductivity of the LWFA, which is still an open issue. There is still no single-shot method of measuring the electron energy evolution [25].

We previously proposed a noninvasive single-shot method to reconstruct the electron acceleration process in Ma *et al.* [26] via a "betatron streaking" concept using x rays from LWFA. During LWFA, electrons perform transverse betatron oscillations due to the inherent transverse focusing force of the plasma wakefield and produce synchrotron-like betatron radiation [7,27,28]. The measurable properties of betatron radiation are completely determined by the electron properties given known plasma parameters. This in turn makes it a powerful tool in revealing the electron properties such as transverse [29–32] and longitudinal [33] beam size, oscillation amplitude [34,35], electron trajectories [36,37] as well as electron injection dynamics [38,39]. In this Letter, we report on the experimental demonstration of single-shot diagnosis of electron energy evolution. By the use of a controlled density gradient, we observed simultaneously the steering of the laser driver, accelerated electron beam as well as the

betatron x-ray beam. The spectrum of the betatron x ray was resolved angularly, which allowed the electron energy evolution to be determined.

The properties of the betatron x rays are correlated with the electron properties. For example, the x-ray critical photon energy and divergence angles can be expressed as [7]

$$E_c = \frac{3}{2}\hbar\omega_\beta K\gamma^2 = \frac{3}{4c}\hbar\omega_p^2 r_\beta \gamma^2,$$
$$\theta_\parallel = K/\gamma = \frac{\omega_p}{c}\frac{r_\beta}{\sqrt{2\gamma}}, \qquad \theta_\perp = 1/\gamma, \tag{1}$$

where $K = \gamma\omega_\beta r_\beta/c$ is the characteristic betatron oscillation strength parameter, $\omega_\beta = \omega_p/\sqrt{2\gamma}$ is the betatron oscillation frequency and $\omega_p = \sqrt{n_p e^2/\varepsilon_0 m_e}$ is the plasma frequency. Thus, the betatron radiation properties are completely determined by the electron energy $\gamma m_e c^2$ and its betatron oscillation amplitude r_β given a known plasma density n_p. Note that the betatron oscillation amplitude r_β scales with electron energy [40], with adiabatic solution $r = r_\beta \sin\psi \simeq r_{\beta 0}(n_0\gamma_0/n_p\gamma)^{1/4}\sin\psi$, where $r_{\beta 0}$, n_0, and γ_0 are the initial betatron oscillation amplitude, plasma density, and particle (normalized) energy, respectively, and ψ is the betatron phase. This means that if we can measure the temporal evolution of the betatron critical energy, we will be able to reconstruct the temporal evolution of the electron acceleration process. Similar to the idea of the synchrotron light source, in which electron bunches at different locations on a circular trajectory emit at different angles, we may use a curved LWFA to convert the temporal evolution of the betatron x ray into an angular distribution [26], i.e., the so-called betatron streaking. Such a curved LWFA is achieved by launching the laser pulse into a plasma with a transverse density gradient in which the laser pulse front tilt develops due to the transverse phase velocity gradient as $v_{pL} = c/\sqrt{1 - n_p/n_c}$. This eventually leads to the laser following a parabolic trajectory.

The experiment was performed on the LWFA-based x-ray beamline at the Advanced Laser Light Source (ALLS) of the Institut National de la Recherche Scientifique (INRS) in Quebec, Canada. The experimental setup is shown in Fig. 1. The laser has a total energy of $E_p \approx 3.2$ J, a full width at half maximum (FWHM) pulse duration of $\tau_p \approx 22$ fs. It was focused by an off-axis parabola (OAP) to a FWHM spot size of 15 μm with a Strehl ratio of 0.8. The pointing stability at focus was $\Delta\theta \approx 2.6$ μrad. During the experiment, real time pointing stability was measured via the leakage of the last turning mirror before the OAP. Correlation of the pointing at focus and through the leakage was performed before the experiment which shows linear correlations in both horizontal and vertical directions. The laser pulse was focused onto a two-stage "T" shaped gas jet target. The first stage (injector) was designed to utilize localized ionization injection with a mixed gas of

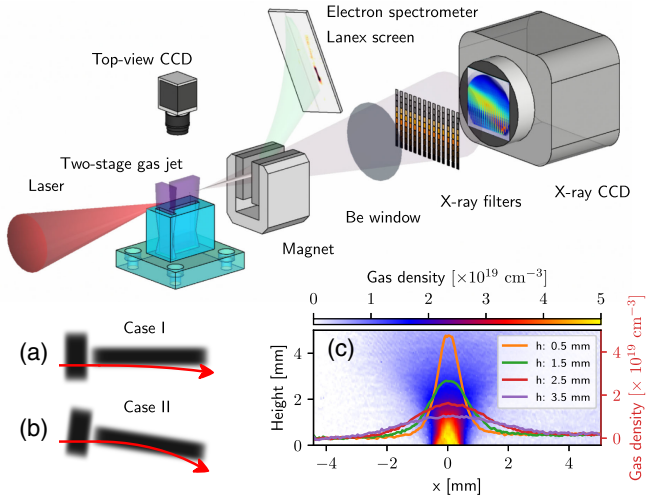

FIG. 1. Experimental setup. A laser pulse was focused on a two-stage gas jet to produce electron and betatron x rays. (a) and (b) The schematic of the laser-target geometry in the two cases, respectively. The red arrows represent the laser trajectories. (c) Measured averaged transverse neutral gas density distribution at a backing pressure of 4.1 MPa and gas density profiles at different heights above the nozzle for the accelerator.

99.5% He + 0.5% N_2 to minimize the energy spread of the electron beam. The second stage (accelerator) was designed to accelerate the injected electron beam but also to provide a quasilinear density gradient at its edges which could be accessed by translating and rotating the gas target. The gas species for the accelerator is pure He. The target was oriented in two configurations, as shown in Figs. 1(a) and 1(b). In the first case, the nozzles are orthogonal to the laser propagation. In the second case, there is a small angle of 25 mrad between the laser incidence and the long edge of the second gas nozzle.

These two-stage gas jets with a configuration similar to that in Ref. [41] were 3D printed using stereolithography (SLA) with the material Acurra 60. The separation of the two stages is 0.5 mm longitudinally. The inner structure of both nozzles is based on the single supersonic nozzle design [42], with parabolic cross section on both sides of the slit throat with a width of 200 μm. The nozzles were controlled independently with solenoid fast pulse valves. The neutral gas density distributions were characterized with a continuous diode laser and a fast gated camera, similar to Ref. [43]. The neutral gas density can reach $n_p \sim 4 \times 10^{19}$ cm^{-3} at a height of 2 mm above the nozzle with a linear dependence with backing pressure. Figure 1(c) shows an example of the measured transverse gas density distribution with a backing pressure of 4.1 MPa. On-shot longitudinal plasma density was measured with a Michelson interferometer.

The laser trajectory was measured by a top-view camera that imaged scattered light along the whole trajectory. The electron beam energy spectrum and pointing in the

horizontal direction were characterized by an electron spectrometer consisting of two removable permanent magnets each with a length of 10 cm and field strength of 1.12 and 0.83 T, respectively. The electron spectrometer measures energies in the range 0.1–1 GeV. The magnetic deflection plane is perpendicular to the transverse density gradient so that the steering of the electron beam has no influence on its energy spectrum measurement. Electrons were measured on a Lanex screen coupled with a CCD camera. The betatron x-ray beam was detected using an x-ray CCD (Princeton Instruments SCX 4300), which was coupled with a $Gd_2O_2S:Tb$ phosphor screen, placed outside of the vacuum chamber with a distance of 1.35 m to the source. The chip size of the CCD is 50 mm × 50 mm and the pixel size is 24 μm. The total acceptance angle of the x-ray CCD is 37 mrad.

An x-ray filter pack, Fig. 1, provided the capability to measure the angularly resolved photon spectrum. The x-ray filters were designed as a 25 × 11 matrix for which each column consists of 11 different thicknesses of aluminum and copper. This pattern repeats 25 times with a 1 mm space between every two neighboring columns to provide a reliable background or beam profile measurement. Each filter element has a dimension of 1 mm × 2 mm. The transmissions of each filter element with the consideration of the quantum efficiency of the CCD as well as the attenuation of the materials such as the Be windows and the air in the beam path were calculated using the mass attenuation coefficients from the NIST x-ray mass attenuation database [44]. The angular resolved x-ray spectrum was retrieved using a forward least-squares fitting method. Each column of the x-ray filter pack gives the x-ray spectrum at a certain angle with an angular resolution of 1.7 mrad. Note that although the intrinsic betatron beam divergence is larger than each filter column subtended angle, we have shown by numerical calculation that this has negligible influence on the inferred betatron spectrum. Figure 3(a) shows raw data from this filter pack diagnostic. The spectral reconstruction procedure involved interpolating from the unfiltered regions to reconstruct the x-ray beam profile. Then, after normalizing the filtered regions using the measured profile, the spectrum can be obtained iteratively, starting from a guessed critical energy E_c of an assumed synchrotronlike spectrum and obtaining the best fit to the transmission of the filter column elements [45,46].

Curved trajectories were observed in the experiment via the top-view CCD. For example, Figs. 2(a) and 2(b) demonstrate the comparison of the laser trajectories in a straight LWFA and a curved LWFA, respectively, by moving the target in the transverse direction. In the former case, the laser propagated in a uniform density region so that the laser trajectories are straight parallel to the edge of the nozzle. While in the latter case, when the target was moved to the very edge of the nozzle where a quasilinear density gradient can be found [see an example in Fig. 1(c)],

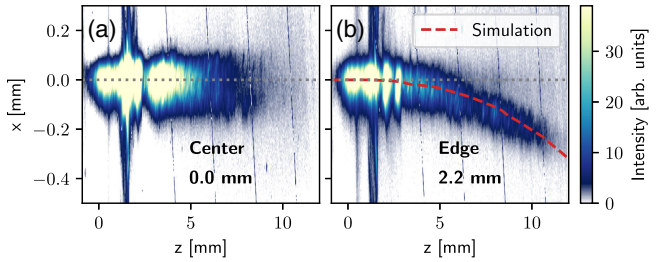

FIG. 2. (a) and (b) Straight and curved laser trajectory examples, respectively, in case I. The labels indicate the centroid of the laser with respect to the center of the gas nozzle at the beginning of the interaction. The red dashed curve in (b) shows the laser trajectory in a PIC simulation for comparison.

the laser pulse was steered gradually during the propagation sideways to form a clear curved trajectory.

A particle-in-cell (PIC) simulation was performed using the 2D OSIRIS code [47]. In the simulation, a Gaussian laser pulse with a normalized intensity $a_0 = 3.1$, a FWHM pulse duration 22 fs, a spot size 15 μm was launched into a two-stage plasma. The first stage included 1% neutral nitrogen in a uniform background plasma of density $n_0 = 3 \times 10^{18}$ cm^{-3}. The second stage was a preionized plasma with a transverse linear density gradient, $dn_p/dx = 6 \times 10^{15}$ cm^{-3}/μm. The density experienced by the center of the laser when entering the second stage is n_0. The maximum deviation of the laser at the end of the propagation was about 300 μm, in excellent agreement with the experimental measurements, as shown in Fig. 2(b).

As a consequence, the streaking of the betatron x rays was realized, as we can see from Fig. 3 as an example, and used it to retrieve the electron acceleration process. First, Fig. 3(a) shows the raw x-ray spatial distribution with the projections of the x-ray filter array. With the method described above, the x-ray critical energy at each angle can be retrieved, which is shown in Fig. 3(b). The correlation of angle to propagation length can be retrieved from the laser trajectory as shown in Fig. 3(c). Here the laser trajectory was fitted with the theoretical model in our previous work [26]. Then, the angle as a function of propagation length can be obtained as the derivative of the parabolic laser trajectory, as shown in Fig. 3(c).

Given that after trapping the electron bunch, its betatron oscillation amplitude depends on the local electron energy and plasma density as $r_\beta \propto [n_p(z)\gamma(z)]^{-1/4}$, the critical energy of the emitted betatron radiation may be written as

$$E_c = \frac{3\hbar e^2}{4\varepsilon_0 m_e c} r_{\beta 0} (n_0\gamma_0)^{1/4} n_p^{3/4} \gamma^{7/4} = C n_p(z)^{3/4} \gamma(z)^{7/4}. \quad (2)$$

As we measured the critical energy as a function of angle θ, which may be converted to z using the Thomson scattering data showing the deflected laser. We also measured the plasma density distribution, as shown in Fig. 3(d). Note that

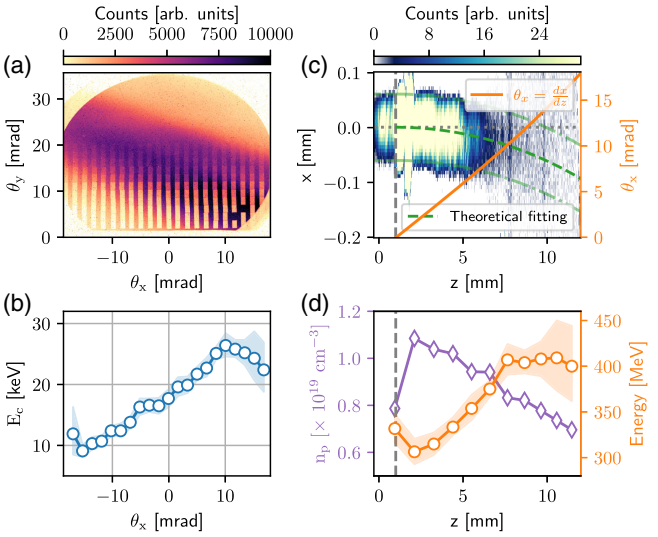

FIG. 3. (a) Raw image of the betatron x-ray profile with the projections of the x-ray filters. (b) Reconstructed betatron x-ray critical energy as a function of angle. (c) A curved laser trajectory for the same shot of (a). The dashed curves were fitted with the theoretical model in Ref. [26]. The solid curve (orange) shows the angle of the laser pointing as a function of laser propagation length taken as the derivative of the laser trajectory. (d) Measured or extrapolated plasma density distribution (purple diamonds) and the reconstructed electron energy (orange circles) as a function of laser propagation length. Note that this example shot is in target orientation case II.

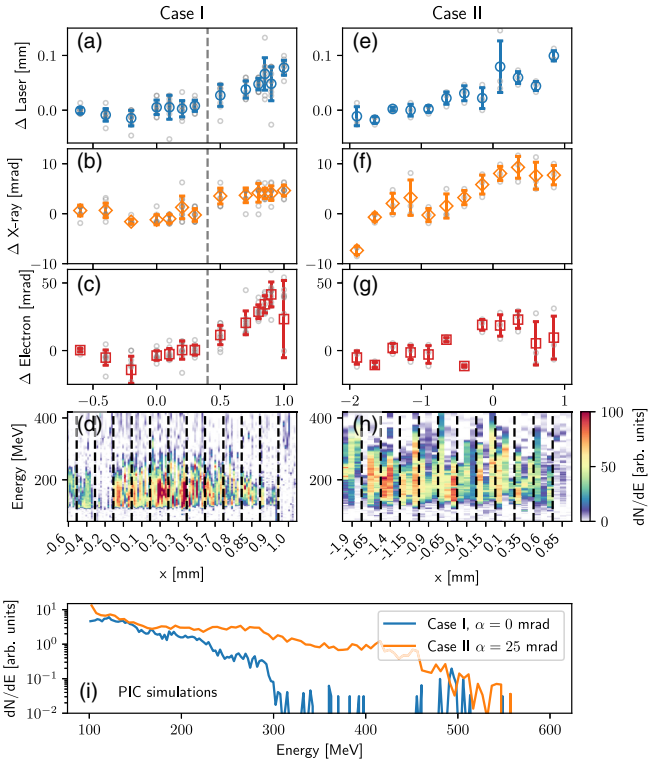

FIG. 4. Steering of the beams in case I (orthogonal incidence) (a)–(c) and case II (grazing incidence) (e)–(g). (a) and (e) The centroid of the laser pulses at the end of the gas nozzle relative to that at the beginning of the gas nozzle. (b) and (f) show the x-ray peak locations relative to the laser axis in vacuum. (c) and (g) The electron beam locations relative to the laser axis in vacuum. The dashed lines in (a)–(c) represent the edge of the accelerator nozzle. (d) and (h)The corresponding electron spectra in the two cases, respectively. In case I (and II), there were 10 (and 3) consecutive shots taken at each condition except for the first data point in case I where 5 shots were taken. (i) The comparison of final electron energy spectra between case I and case II in PIC simulations.

because the field-of-view of the interferometry detector only covered the first 8 mm of the gas target, the last four data points shown were extrapolated. We then may invert Eq. (2) to obtain the z dependence of the electron bunch energy, $\gamma(z) = (E_c/C)^{4/7} n_p^{-3/7}$. The initial conditions for the betatron oscillations are complicated and depend on the particle injection, etc., so the constant C in this expression is difficult to know *a priori*. However, as the electron energy at the end of the interaction γ_1, the corresponding critical energy of the betatron x ray E_{c1} and the plasma density n_{p1} have been measured, we can simply fit to these, assuming an electron bunch with energy $\gamma(z)$ and uncorrelated transverse oscillations of average initial width $r_{\beta 0}$. Note that numerical calculations have shown that a Gaussian energy spread about $\gamma(z)$ has negligible influence on the betatron spectrum compared to a monoenergetic peak. Thus, the evolution of the electron energy can be determined as

$$\gamma(z) = \left[\frac{E_c(\theta(z))}{E_{c1}}\right]^{4/7} \left[\frac{n_{p1}}{n_p(z)}\right]^{3/7} \gamma_1. \tag{3}$$

Using the initial condition, i.e., the final electron energy and the betatron x-ray critical energy at the corresponding angle as well as the measured plasma density distribution, the evolution of the electron energy can be reconstructed which is shown in Fig. 3(d). Note that the temporal resolution of electron energy evolution is determined by the angular resolution of the x-ray filter pack and the particular curved laser trajectories. For this example shot, the temporal resolution is about 3.7 ps which corresponds to a 1.1 mm spatial step.

In this work, we also demonstrated quantitative measurements of steering of the laser, electron, and x-ray beams, as given in Fig. 4. We investigated such steering in two scenarios of the gas target orientation, as shown in Figs. 1(a) and 1(b). In case I, the nozzles are parallel to the laser propagation direction. Therefore, when scanning the transverse location of the target, the laser pulse experienced regions with either uniform plasma density or with linear density gradient. Consequently, the laser displacement, the betatron x-ray beam and the electron beam pointing all demonstrate a plateau followed by a linear transition starting at approximately $x = 0.4$ mm,

as shown in Figs. 4(a)–4(c). In case II, there is a small angle of 25 mrad between the laser direction and the long edge of the second gas nozzle such that the laser will always experience a transverse density gradient regardless of the initial transverse location. Hence, the plateau observed in case I does not appear; all three beams were steered consistently, as we can see from Figs. 4(e)–4(g). Figures 4(d) and 4(h) show the electron spectra in the two cases, respectively. In case I, the change in the maximum electron energy follows the same general trend as the beam steering. The maximum electron energy gain in case II is in general higher than that in case I, which indicates the realization of rephasing [26,48–52] because the laser experienced a density up ramp. As the plasma density increases, the plasma wavelength decreases, which shrinks the wakefield period, keeping the electron beam in the accelerating phase longer and eventually resulting in a higher final energy gain. The energy gain enhancement due to rephasing was confirmed qualitatively by PIC simulations, as shown in Fig. 4(i). Here, the laser parameters were the same as the simulation in Fig. 2(b). The plasma density was $n_0 = 1.5 \times 10^{18}$ cm^{-3}. The second stage was a pure electron plasma with a linear transverse density gradient, $dn_p/dx = 3 \times 10^{15}$ cm^{-3}/μm. Note that in case II, the plasma density gradient direction was tilted by 25 mrad while maintaining the same initial density experienced by the laser pulse when entering the second stage.

In summary, we have demonstrated experimentally the streaking of betatron x rays and utilized it for retrieving the electron acceleration process in LWFA in a single-shot mode. Such a streaking technique was realized with a linear transverse density gradient in which the LWFA drive laser propagates in a parabolic trajectory.

Our work could find applications in advanced control of laser beam and particle propagation, such as generating curved plasma channel [53] for LWFA in pre-formed curved plasma channel [54] and for coupling multistage LWFA as proposed in Ref. [55] as well as enabling compact synchrotron sources [56]. Moreover, the angular streaked betatron x ray has an intrinsic spatiotemporal correlation, which makes it a promising tool for single-shot pump-probe applications.

This work was supported by DOE Office of Science, Fusion Energy Sciences under Contract No. DE-SC0021246: the LaserNetUS initiative at Advanced Laser Light Source; DOE Grant No. DE-SC0022109, NSF Grant No. 2108075, 2126181, 1935950 and DOE Grant No. DE-SC0020237. This work was also supported by the European Research Council (ERC) under the European Union's Horizon 2020 research and innovation programme (Grant Agreement No. 682399) and the John Adams Institute for Accelerator Science (STFC: ST/V001639/1). The authors also acknowledge support from Canada Foundation for Innovation—Major Science Initiatives and MEIE. M. J. V. S. acknowledges support from the Royal Society URF-R1221874. A. E. H. acknowledges support from the Natural Sciences and Engineering Research Council of Canada (Grant No. RGPIN-2021-04373). The authors would like to acknowledge the OSIRIS Consortium, consisting of University of California, Los Angeles (USA) and Instituto Superior Ténico (Lisbon, Portugal) for the use of the OSIRIS4.0 framework. The authors would also like to thank Joël Maltais, Stéphane Payeur, Claude Sirois, François Légaré from ALLS for technical support.

*yongm@umich.edu

[1] T. Tajima and J. M. Dawson, Laser electron accelerator, Phys. Rev. Lett. **43**, 267 (1979).

[2] A. J. Gonsalves, K. Nakamura, J. Daniels, C. Benedetti, C. Pieronek, T. C. H. de Raadt, S. Steinke, J. H. Bin, S. S. Bulanov, J. van Tilborg, C. G. R. Geddes, C. B. Schroeder, C. Tóth, E. Esarey, K. Swanson, L. Fan-Chiang, G. Bagdasarov, N. Bobrova, V. Gasilov, G. Korn, P. Sasorov, and W. P. Leemans, Petawatt laser guiding and electron beam acceleration to 8 gev in a laser-heated capillary discharge waveguide, Phys. Rev. Lett. **122**, 084801 (2019).

[3] B. Miao, J. E. Shrock, L. Feder, R. C. Hollinger, J. Morrison, R. Nedbailo, A. Picksley, H. Song, S. Wang, J. J. Rocca, and H. M. Milchberg, Multi-gev electron bunches from an all-optical laser wakefield accelerator, Phys. Rev. X **12**, 031038 (2022).

[4] W. P. Leemans, A. J. Gonsalves, H.-S. Mao, K. Nakamura, C. Benedetti, C. B. Schroeder, C. Tóth, J. Daniels, D. E. Mittelberger, S. S. Bulanov, J.-L. Vay, C. G. R. Geddes, and E. Esarey, Multi-gev electron beams from capillary-discharge-guided subpetawatt laser pulses in the self-trapping regime, Phys. Rev. Lett. **113**, 245002 (2014).

[5] X. Wang, R. Zgadzaj, N. Fazel, Z. Li, S. A. Yi, X. Zhang, W. Henderson, Y. Y. Chang, R. Korzekwa, H. E. Tsai, C. H. Pai, H. Quevedo, G. Dyer, E. Gaul, M. Martinez, A. C. Bernstein, T. Borger, M. Spinks, M. Donovan, V. Khudik, G. Shvets, T. Ditmire, and M. C. Downer, Quasi-monoenergetic laser-plasma acceleration of electrons to 2 gev, Nat. Commun. **4**, 1988 (2013).

[6] H. T. Kim, K. H. Pae, H. J. Cha, I. J. Kim, T. J. Yu, J. H. Sung, S. K. Lee, T. M. Jeong, and J. Lee, Enhancement of electron energy to the multi-gev regime by a dual-stage laser-wakefield accelerator pumped by petawatt laser pulses, Phys. Rev. Lett. **111**, 165002 (2013).

[7] S. Corde, K. Ta Phuoc, G. Lambert, R. Fitour, V. Malka, A. Rousse, A. Beck, and E. Lefebvre, Femtosecond x rays from laser-plasma accelerators, Rev. Mod. Phys. **85**, 1 (2013).

[8] F. Albert and A. G. R. Thomas, Applications of laser wakefield accelerator-based light sources, Plasma Phys. Controlled Fusion **58**, 103001 (2016).

[9] W. Wang, K. Feng, L. Ke, C. Yu, Y. Xu, R. Qi, Y. Chen, Z. Qin, Z. Zhang, M. Fang, J. Liu, K. Jiang, H. Wang, C. Wang, X. Yang, F. Wu, Y. Leng, J. Liu, R. Li, and Z. Xu, Free-electron lasing at 27 nanometres based on a laser wakefield accelerator, Nature (London) **595**, 516 (2021).

[10] C. Emma, J. Van Tilborg, R. Assmann, S. Barber, A. Cianchi, S. Corde, M. E. Couprie, R. D'Arcy, M. Ferrario, A. F. Habib *et al.*, Free electron lasers driven by plasma accelerators: Status and near-term prospects, High Power Laser Sci. Eng. **9**, e57 (2021).

[11] J. M. Cole, K. T. Behm, E. Gerstmayr, T. G. Blackburn, J. C. Wood, C. D. Baird, M. J. Duff, C. Harvey, A. Ilderton, A. S. Joglekar, K. Krushelnick, S. Kuschel, M. Marklund, P. McKenna, C. D. Murphy, K. Poder, C. P. Ridgers, G. M. Samarin, G. Sarri, D. R. Symes, A. G. R. Thomas, J. Warwick, M. Zepf, Z. Najmudin, and S. P. D. Mangles, Experimental evidence of radiation reaction in the collision of a high-intensity laser pulse with a laser-wakefield accelerated electron beam, Phys. Rev. X **8**, 011020 (2018).

[12] K. Poder, M. Tamburini, G. Sarri, A. Di Piazza, S. Kuschel, C. D. Baird, K. Behm, S. Bohlen, J. M. Cole, D. J. Corvan, M. Duff, E. Gerstmayr, C. H. Keitel, K. Krushelnick, S. P. D. Mangles, P. McKenna, C. D. Murphy, Z. Najmudin, C. P. Ridgers, G. M. Samarin, D. R. Symes, A. G. R. Thomas, J. Warwick, and M. Zepf, Experimental signatures of the quantum nature of radiation reaction in the field of an ultraintense laser, Phys. Rev. X **8**, 031004 (2018).

[13] A. G. R. Thomas and D. Seipt, Modeling chromatic emittance growth in staged plasma wakefield acceleration to 1 tev using nonlinear transfer matrices, Phys. Rev. Accel. Beams **24**, 104602 (2021).

[14] E. Esarey, C. B. Schroeder, and W. P. Leemans, Physics of laser-driven plasma-based electron accelerators, Rev. Mod. Phys. **81**, 1229 (2009).

[15] W. Leemans and E. Esarey, Laser-driven plasma-wave electron accelerators, Phys. Today, No. 3, **62**, 44 (2009).

[16] J. P. Palastro, J. L. Shaw, P. Franke, D. Ramsey, T. T. Simpson, and D. H. Froula, Dephasingless laser wakefield acceleration, Phys. Rev. Lett. **124**, 134802 (2020).

[17] C. Caizergues, S. Smartsev, V. Malka, and C. Thaury, Phase-locked laser-wakefield electron acceleration, Nat. Photonics **14**, 475 (2020).

[18] A. Debus, R. Pausch, A. Huebl, K. Steiniger, R. Widera, T. E. Cowan, U. Schramm, and M. Bussmann, Circumventing the dephasing and depletion limits of laser-wakefield acceleration, Phys. Rev. X **9**, 031044 (2019).

[19] J. Faure, C. Rechatin, A. Norlin, A. Lifschitz, Y. Glinec, and V. Malka, Controlled injection and acceleration of electrons in plasma wakefields by colliding laser pulses, Nature (London) **444**, 737 (2006).

[20] A. Buck, J. Wenz, J. Xu, K. Khrennikov, K. Schmid, M. Heigoldt, J. M. Mikhailova, M. Geissler, B. Shen, F. Krausz, S. Karsch, and L. Veisz, Shock-front injector for high-quality laser-plasma acceleration, Phys. Rev. Lett. **110**, 185006 (2013).

[21] W. T. Wang, W. T. Li, J. S. Liu, Z. J. Zhang, R. Qi, C. H. Yu, J. Q. Liu, M. Fang, Z. Y. Qin, C. Wang, Y. Xu, F. X. Wu, Y. X. Leng, R. X. Li, and Z. Z. Xu, High-brightness high-energy electron beams from a laser wakefield accelerator via energy chirp control, Phys. Rev. Lett. **117**, 124801 (2016).

[22] K. K. Swanson, H.-E. Tsai, S. K. Barber, R. Lehe, H.-S. Mao, S. Steinke, J. van Tilborg, K. Nakamura, C. G. R. Geddes, C. B. Schroeder, E. Esarey, and W. P. Leemans, Control of tunable, monoenergetic laser-plasma-accelerated electron beams using a shock-induced density downramp injector, Phys. Rev. Accel. Beams **20**, 051301 (2017).

[23] D. E. Cardenas, S. Chou, E. Wallin, J. Xu, L. Hofmann, A. Buck, K. Schmid, D. E. Rivas, B. Shen, A. Gonoskov, M. Marklund, and L. Veisz, Electron bunch evolution in laser-wakefield acceleration, Phys. Rev. Accel. Beams **23**, 112803 (2020).

[24] S. Bohlen, T. Brümmer, F. Grüner, C. A. Lindstrøm, M. Meisel, T. Staufer, M. J. V. Streeter, M. C. Veale, J. C. Wood, R. D'Arcy, K. Põder, and J. Osterhoff, In situ measurement of electron energy evolution in a laser-plasma accelerator, Phys. Rev. Lett. **129**, 244801 (2022).

[25] M. C. Downer, R. Zgadzaj, A. Debus, U. Schramm, and M. C. Kaluza, Diagnostics for plasma-based electron accelerators, Rev. Mod. Phys. **90**, 035002 (2018).

[26] Y. Ma, D. Seipt, S. J. D. Dann, M. J. V. Streeter, C. A. J. Palmer, L. Willingale, and A. G. R. Thomas, Angular streaking of betatron x-rays in a transverse density gradient laser-wakefield accelerator, Phys. Plasmas **25**, 113105 (2018).

[27] E. Esarey, B. A. Shadwick, P. Catravas, and W. P. Leemans, Synchrotron radiation from electron beams in plasma-focusing channels, Phys. Rev. E **65**, 056505 (2002).

[28] A. G. R. Thomas and K. Krushelnick, Betatron x-ray generation from electrons accelerated in a plasma cavity in the presence of laser fields, Phys. Plasmas **16**, 103103 (2009).

[29] S. Kneip, C. McGuffey, J. L. Martins, M. S. Bloom, V. Chvykov, F. Dollar, R. Fonseca, S. Jolly, G. Kalintchenko, K. Krushelnick, A. Maksimchuk, S. P. D. Mangles, Z. Najmudin, C. A. J. Palmer, K. T. Phuoc, W. Schumaker, L. O. Silva, J. Vieira, V. Yanovsky, and A. G. R. Thomas, Characterization of transverse beam emittance of electrons from a laser-plasma wakefield accelerator in the bubble regime using betatron x-ray radiation, Phys. Rev. ST Accel. Beams **15**, 021302 (2012).

[30] G. R. Plateau, C. G. R. Geddes, D. B. Thorn, M. Chen, C. Benedetti, E. Esarey, A. J. Gonsalves, N. H. Matlis, K. Nakamura, C. B. Schroeder, S. Shiraishi, T. Sokollik, J. van Tilborg, C. Toth, S. Trotsenko, T. S. Kim, M. Battaglia, T. Stöhlker, and W. P. Leemans, Low-emittance electron bunches from a laser-plasma accelerator measured using single-shot x-ray spectroscopy, Phys. Rev. Lett. **109**, 064802 (2012).

[31] A. Köhler, J. Couperus, O. Zarini, A. Jochmann, A. Irman, and U. Schramm, Single-shot betatron source size measurement from a laser-wakefield accelerator, Nucl. Instrum. Methods Phys. Res., Sect. A **829**, 265 (2016).

[32] A. Curcio, M. Anania, F. Bisesto, E. Chiadroni, A. Cianchi, M. Ferrario, F. Filippi, D. Giulietti, A. Marocchino, M. Petrarca, V. Shpakov, and A. Zigler, Trace-space reconstruction of low-emittance electron beams through betatron radiation in laser-plasma accelerators, Phys. Rev. Accel. Beams **20**, 012801 (2017).

[33] S. Corde, C. Thaury, K. T. Phuoc, A. Lifschitz, G. Lambert, J. Faure, O. Lundh, E. Benveniste, A. Ben-Ismail, L. Arantchuk, A. Marciniak, A. Stordeur, P. Brijesh, A. Rousse, A. Specka, and V. Malka, Mapping the x-ray emission region in a laser-plasma accelerator, Phys. Rev. Lett. **107**, 215004 (2011).

[34] F. Albert, R. Shah, K. T. Phuoc, R. Fitour, F. Burgy, J.-P. Rousseau, A. Tafzi, D. Douillet, T. Lefrou, and A. Rousse, Betatron oscillations of electrons accelerated in laser wakefields characterized by spectral x-ray analysis, Phys. Rev. E **77**, 056402 (2008).

[35] M. Schnell, A. Sävert, B. Landgraf, M. Reuter, M. Nicolai, O. Jäckel, C. Peth, T. Thiele, O. Jansen, A. Pukhov, O. Willi, M. C. Kaluza, and C. Spielmann, Deducing the electron-beam diameter in a laser-plasma accelerator using x-ray betatron radiation, Phys. Rev. Lett. **108**, 075001 (2012).

[36] K. Ta Phuoc, S. Corde, R. Shah, F. Albert, R. Fitour, J.-P. Rousseau, F. Burgy, B. Mercier, and A. Rousse, Imaging electron trajectories in a laser-wakefield cavity using betatron x-ray radiation, Phys. Rev. Lett. **97**, 225002 (2006).

[37] F. Albert, B. B. Pollock, J. L. Shaw, K. A. Marsh, J. E. Ralph, Y.-H. Chen, D. Alessi, A. Pak, C. E. Clayton, S. H. Glenzer, and C. Joshi, Angular dependence of betatron x-ray spectra from a laser-wakefield accelerator, Phys. Rev. Lett. **111**, 235004 (2013).

[38] S. P. D. Mangles, G. Genoud, S. Kneip, M. Burza, K. Cassou, B. Cros, N. P. Dover, C. Kamperidis, Z. Najmudin, A. Persson, J. Schreiber, F. Wojda, and C.-G. Wahlström, Controlling the spectrum of x-rays generated in a laser-plasma accelerator by tailoring the laser wavefront, Appl. Phys. Lett. **95**, 181106 (2009).

[39] S. Corde, C. Thaury, A. Lifschitz, G. Lambert, K. Ta Phuoc, X. Davoine, R. Lehe, D. Douillet, A. Rousse, and V. Malka, Observation of longitudinal and transverse self-injections in laser-plasma accelerators, Nat. Commun. **4**, 1501 (2013).

[40] A. G. R. Thomas, Scalings for radiation from plasma bubbles, Phys. Plasmas **17**, 056708 (2010).

[41] G. Golovin, S. Chen, N. Powers, C. Liu, S. Banerjee, J. Zhang, M. Zeng, Z. Sheng, and D. Umstadter, Tunable monoenergetic electron beams from independently controllable laser-wakefield acceleration and injection, Phys. Rev. ST Accel. Beams **18**, 011301 (2015).

[42] T. Hosokai, K. Kinoshita, T. Watanabe, K. Yoshii, T. Ueda, A. Zhidokov, M. Uesaka, K. Nakajima, M. Kando, and H. Kotaki, Supersonic gas jet target for generation of relativistic electrons with 12-TW 50-fs laser pulse, in *Proceedings of the 8th European Particle Accelerator Conference (EPAC 2002)* (2002), pp. 981–983.

[43] V. Malka, C. Coulaud, J. P. Geindre, V. Lopez, Z. Najmudin, D. Neely, and F. Amiranoff, Characterization of neutral density profile in a wide range of pressure of cylindrical pulsed gas jets, Rev. Sci. Instrum. **71**, 2329 (2000).

[44] J. H. Hubbell and S. M. Seltzer, Nist standard reference database 126: Tables of x-ray mass attenuation coefficients and mass energy-absorption coefficients from 1 kev to 20 mev for elements $z = 1$ to 92 and 48 additional substances of dosimetric interest, 10.18434/T4D01F.

[45] J. C. Wood, Betatron radiation from laser wakefield accelerators and its applications, Ph.D. dissertation, Imperial College London, 2016.

[46] A. E. Hussein *et al.*, Laser-wakefield accelerators for high-resolution x-ray imaging of complex microstructures, Sci. Rep. **9**, 3249 (2019).

[47] R. A. Fonseca, L. O. Silva, F. S. Tsung, V. K. Decyk, W. Lu, C. Ren, W. B. Mori, S. Deng, S. Lee, T. Katsouleas, and J. C. Adam, OSIRIS: A three-dimensional, fully relativistic particle in cell code for modeling plasma based accelerators, in *Computational Science—ICCS 2002*, edited by P. M. A. Sloot, A. G. Hoekstra, C. J. K. Tan, and J. J. Dongarra (Springer Berlin Heidelberg, Berlin, Heidelberg, 2002), pp. 342–351.

[48] S. V. Bulanov, V. A. Vshivkov, G. I. Dudnikova, F. Naumova, N M anbd Pegoraro, and I. V. Pogorelsky, Laser acceleration of charged particles in inhomogeneous plasmas i, Plasma Phys. Rep. **23**, 259 (1997).

[49] P. Sprangle, B. Hafizi, J. R. Peñano, R. F. Hubbard, A. Ting, C. I. Moore, D. F. Gordon, A. Zigler, D. Kaganovich, and T. M. Antonsen, Wakefield generation and gev acceleration in tapered plasma channels, Phys. Rev. E **63**, 056405 (2001).

[50] A. Pukhov and I. Kostyukov, Control of laser-wakefield acceleration by the plasma-density profile, Phys. Rev. E **77**, 025401(R) (2008).

[51] E. Guillaume, A. Döpp, C. Thaury, K. Ta Phuoc, A. Lifschitz, G. Grittani, J.-P. Goddet, A. Tafzi, S. W. Chou, L. Veisz, and V. Malka, Electron rephasing in a laser-wakefield accelerator, Phys. Rev. Lett. **115**, 155002 (2015).

[52] M. Kozlova, I. Andriyash, J. Gautier, S. Sebban, S. Smartsev, N. Jourdain, U. Chaulagain, Y. Azamoum, A. Tafzi, J.-P. Goddet, K. Oubrerie, C. Thaury, A. Rousse, and K. Ta Phuoc, Hard x rays from laser-wakefield accelerators in density tailored plasmas, Phys. Rev. X **10**, 011061 (2020).

[53] Y. Ma, D. Seipt, K. Krushelnick, and A. G. R. Thomas, Generation of straight and curved hollow plasma channels by laser-generated nonlinear wakefields and studies of ultra-intense laser pulse guiding, Phys. Plasmas **28**, 063104 (2021).

[54] X. Zhu, B. Li, F. Liu, J. Li, Z. Bi, X. Ge, H. Deng, Z. Zhang, P. Cui, L. Lu, W. Yan, X. Yuan, L. Chen, Q. Cao, Z. Liu, Z. Sheng, M. Chen, and J. Zhang, Experimental demonstration of laser guiding and wakefield acceleration in a curved plasma channel, Phys. Rev. Lett. **130**, 215001 (2023).

[55] J. Luo, M. Chen, W. Y. Wu, S. M. Weng, Z. M. Sheng, C. B. Schroeder, D. A. Jaroszynski, E. Esarey, W. P. Leemans, W. B. Mori, and J. Zhang, Multistage coupling of laser-wakefield accelerators with curved plasma channels, Phys. Rev. Lett. **120**, 154801 (2018).

[56] M. Chen, J. Luo, F.-Y. Li, F. Liu, Z.-M. Sheng, and J. Zhang, Tunable synchrotron-like radiation from centimeter scale plasma channels, Light Sci. Appl. **5**, e16015 (2016).